J. Fluid Mech. (2000), *vol.* 406, *pp.* 55–80. Printed in the United Kingdom

Aerosol particle transport and deposition in vertical and horizontal turbulent duct flows

By HAIFENG ZHANG AND GOODARZ AHMADI

Department of Mechanical and Aeronautical Engineering,
Clarkson University, Potsdam, NY 13699, USA

(Received 3 April 1998 and in revised form 22 July 1999)

Aerosol particle transport and deposition in vertical and horizontal turbulent duct flows in the presence of different gravity directions are studied. The instantaneous fluid velocity field is generated by the direct numerical simulation of the Navier–Stokes equation via a pseudospectral method. A particle equation of motion including Stokes drag, Brownian diffusion, lift and gravitational forces is used for trajectory analysis. Ensembles of 8192 particle paths are evaluated, compiled, and statistically analysed. The results show that the wall coherent structure plays an important role in the particle deposition process. The simulated deposition velocities under various conditions are compared with the available experimental data and the sublayer model predictions. It is shown that the shear velocity, density ratio, the shear-induced lift force and the flow direction affect the particle deposition rate. The results for vertical ducts show that the particle deposition velocity varies with the direction of gravity, and the effect becomes more significant when the shear velocity is small. For horizontal ducts, the gravitational sedimentation increases the particle deposition rate on the lower wall.

1. Introduction

Study of transport and deposition of aerosols has attracted considerable attention due to its importance in numerous industrial applications. Particle transport and deposition play a major role in filtration, combustion, air and water pollution, coal transport and cleaning, microcontamination control, xerography, and many other industrial processes.

Extensive experimental and computational studies related to particle transport in turbulent flows have been reported in the literature (Hinze 1975; Hinds 1982; Ahmadi 1993; Wood 1981*b*; Papavergos & Hedley 1984). McCoy & Hanratty (1977) reviewed experimental measurements of the deposition rate of particles and droplets in vertical pipes containing turbulent gas flows, and they suggested a correlation based on the value of the particle relaxation time in wall units. A sublayer model for particle resuspension and deposition in turbulent flows was proposed by Cleaver & Yates (1973, 1975, 1976), Fichman, Gutfinger & Pnueli (1988) and Fan & Ahmadi (1993). In the last work, the effect of wall roughness was included, and an empirical equation for particle deposition rate was proposed.

Direct numerical simulations (DNS) of particle deposition in wall-bounded turbulent flows were performed by McLaughin (1989) and Ounis, Ahmadi & McLaughlin (1991, 1993). These studies were concerned with clarifying the particle deposition mechanisms. Brooke *et al.* (1992) performed detailed DNS studies of vortical structures in the viscous sublayer. Recently, Pendinotti, Mariotti & Banerjee (1992) used

DNS to investigate the particle behaviour in the wall region of turbulent flows. They reported that an initially uniform distribution of particles tends to segregate into low-speed streaks and resuspension occurs by particles being ejected from the wall. DNS simulation was used by Soltani & Ahmadi (1995) to study the particle entrainment process in a turbulent channel flow. They found that the wall coherent structure plays a dominant role on the particle entrainment process.

Squires & Eaton (1991*a*) simulated a homogeneous isotropic non-decaying turbulent flow field by imposing an excitation at low wavenumbers, and studied the effects of inertia on particle dispersion. They also used the DNS procedure to study the preferential micro-concentration structure of particles as a function of Stokes number in turbulent near-wall flows (Squires & Eaton 1991*b*). Rashidi, Hetsroni & Banerjee (1990) performed an experiment to study the particle–turbulence interactions near a wall. They reported that particle transport is mainly controlled by burst phenomena.

In this work, aerosol deposition from turbulent air streams in vertical and horizontal ducts is studied. The turbulent flow field is generated by the direct numerical simulation of the Navier–Stokes equation. The Stokes drag force, lift force, Brownian force and gravitational force are included in the simulation. The predicted deposition velocities under various conditions are compared with the available experimental data and empirical equations. It is shown that the particle-to-fluid density ratio, the shear-induced lift force, the flow direction and the shear velocity affect the particle deposition rate. For both vertical and horizontal ducts, the DNS results show that the effect of gravity and its direction on the particle deposition rate becomes more significant at low shear velocities.

2. Turbulent flow field velocity

The instantaneous fluid velocity field in the channel is evaluated by DNS of the Navier–Stokes equation. It is assumed that the fluid is incompressible, and a constant mean pressure gradient in the x-direction is imposed. The corresponding governing equations of motion are

$$\nabla \cdot \boldsymbol{V}^f = 0, \tag{1}$$

$$\frac{\partial \boldsymbol{V}^f}{\partial t} + \boldsymbol{V}^f \cdot \nabla \boldsymbol{V}^f = \nu \nabla^2 \boldsymbol{V}^f - \frac{1}{\rho^f} \nabla P, \tag{2}$$

where $\boldsymbol{V}^f$ is the fluid velocity vector, P is the pressure, ρ^f is the density, and ν is the kinematic viscosity. The fluid velocity is assumed to satisfy the no-slip boundary conditions at the channel walls. In wall units, the channel has a width of 250, and a 630×630 periodic segment in the x- and z-directions is used in the simulations. A $16 \times 64 \times 64$ computational grid in the (x, y, z)-directions is also used in most of the computations. The grid spacings in the x- and z-directions are constant, while the variation of grid points in the y-direction is represented by the Chebyshev series. The distance of the ith grid point in the y-direction from the centreline is given as

$$y_i = \tfrac{1}{2} h \cos(\pi \mathrm{i}/M), \quad 0 \leqslant \mathrm{i} \leqslant M. \tag{3}$$

Here $M = 64$, and there are 65 grid points in the y-direction. The flow field is also evaluated using finer grids, and the results are compared.

The channel flow code used in this study is the one developed by McLaughlin (1989). To solve for the velocity components by pseudospectral methods, the fluid velocity is expanded in a three-dimensional Fourier–Chebyshev series. Variations of

the fluid velocity field in the x- and z-directions are given by Fourier series, while in the y-direction the Chebyshev series are used. The code uses an Adams–Bashforth–Crank–Nickelson (ABCN) scheme to compute the nonlinear and viscous terms in the Navier–Stokes equation and performs three fractional time steps to forward the fluid velocity from time step (N_t) to time step ($N_t + 1$). These steps account for the nonlinear term and the pressure terms. In the computational model, the nonlinear terms are evaluated with second-order accuracy in Δt as

$$\boldsymbol{V}^f_{(N+1/3)} = \boldsymbol{V}^f_{(N)} - \left(\frac{\mathrm{d}p_{ext}}{\mathrm{d}x}\right)\Delta t\,\hat{\boldsymbol{x}} - \frac{U(y)}{2}\left(\frac{\partial \boldsymbol{V}^f_{(N+1/3)}}{\partial x} + \frac{\partial \boldsymbol{V}^f_{(N-2/3)}}{\partial x}\right)\Delta t + \tfrac{3}{2}\boldsymbol{F}_{(N-2/3)} - \tfrac{1}{2}\boldsymbol{F}_{(N-5/3)}, \tag{4}$$

where

$$\boldsymbol{F} = \left(\boldsymbol{V}^f \times \boldsymbol{\omega} + U(y)\frac{\partial \boldsymbol{V}^f}{\partial x}\right)\Delta t. \tag{5}$$

In (4) and (5), $U(y)$ is a fit to the mean velocity profile, $\hat{\boldsymbol{x}}$ is the unit vector in the x-direction, $\mathrm{d}p_{ext}/\mathrm{d}x$ is the pressure gradient, and $\boldsymbol{\omega} = \nabla \times \boldsymbol{V}^f$ is the vorticity vector. Here the subscripts $N + 1/3$, $N - 2/3$, and $N - 5/3$ stand for values evaluated at different fraction steps.

To apply the correct viscous boundary conditions on the pressure near the wall, the pressure term is divided into inviscid, p_i and viscous, p_v, which satisfy the following equations:

$$\nabla^2 p_{i(N+1)} = \frac{1}{\Delta t}\nabla \cdot \boldsymbol{V}^f_{(N+1/3)}, \quad \nabla^2 p_{v(N+1)} = 0. \tag{6}$$

The boundary conditions are given by

$$\frac{\partial p_{i(N+1)}}{\partial y} = 0, \quad \frac{\partial^2 p_{v(N+1)}}{\partial y^2} = \frac{\partial^2 u^f_{(N+1)}}{\partial y^2} \quad \text{at} \quad y = \pm\frac{h}{2}. \tag{7}$$

The velocities at the second and the third fractional time steps are computed by

$$\boldsymbol{V}^f_{(N+2/3)} = \boldsymbol{V}^f_{(N+1/3)} - \Delta t \nabla p_{i(N+1)} \tag{8}$$

and

$$\boldsymbol{V}^f_{(N+1)} = \boldsymbol{V}^f_{(N+2/3)} + \Delta t \nabla^2 \boldsymbol{V}^f_{(N+1)} - \Delta t \nabla p_{v(N+1)}. \tag{9}$$

Since the velocity at time step ($N + 1$), $\boldsymbol{V}^f_{(N+1)}$, appears on the right-hand side of (9), (6)–(9) must be solved simultaneously. For that purpose, p_v is first expanded in a set of Green's functions as described by Marcus (1984). Pseudospectral methods are then used to solve for the velocity components. Additional details of the numerical techniques were described by McLaughlin (1989). In simulations, wall units are used; and all variables are non-dimensionalized in terms of shear velocity u^* and kinematic viscosity ν.

Figure 1 shows a sample instantaneous velocity field at $t^+ = 100$ in different planes. While the velocity field in the (y, z)-plane (at $x^+ = 157.5$) shown in figure 1(a) has a random pattern, near-wall coherent eddies and flow streams towards and away from the wall can be observed in this figure. Figure 1(b) shows the velocity vector plot in the (x, y)-plane (at $z^+ = 157.5$). The random deviations from the expected mean velocity profile are clearly seen. The velocity field in the (x, z)-plane (at $y^+ = 88.4$) shown in figure 1(c) indicates that the flow is predominantly in the x-direction. The low- and high-speed streaks are also noticeable in this figure.

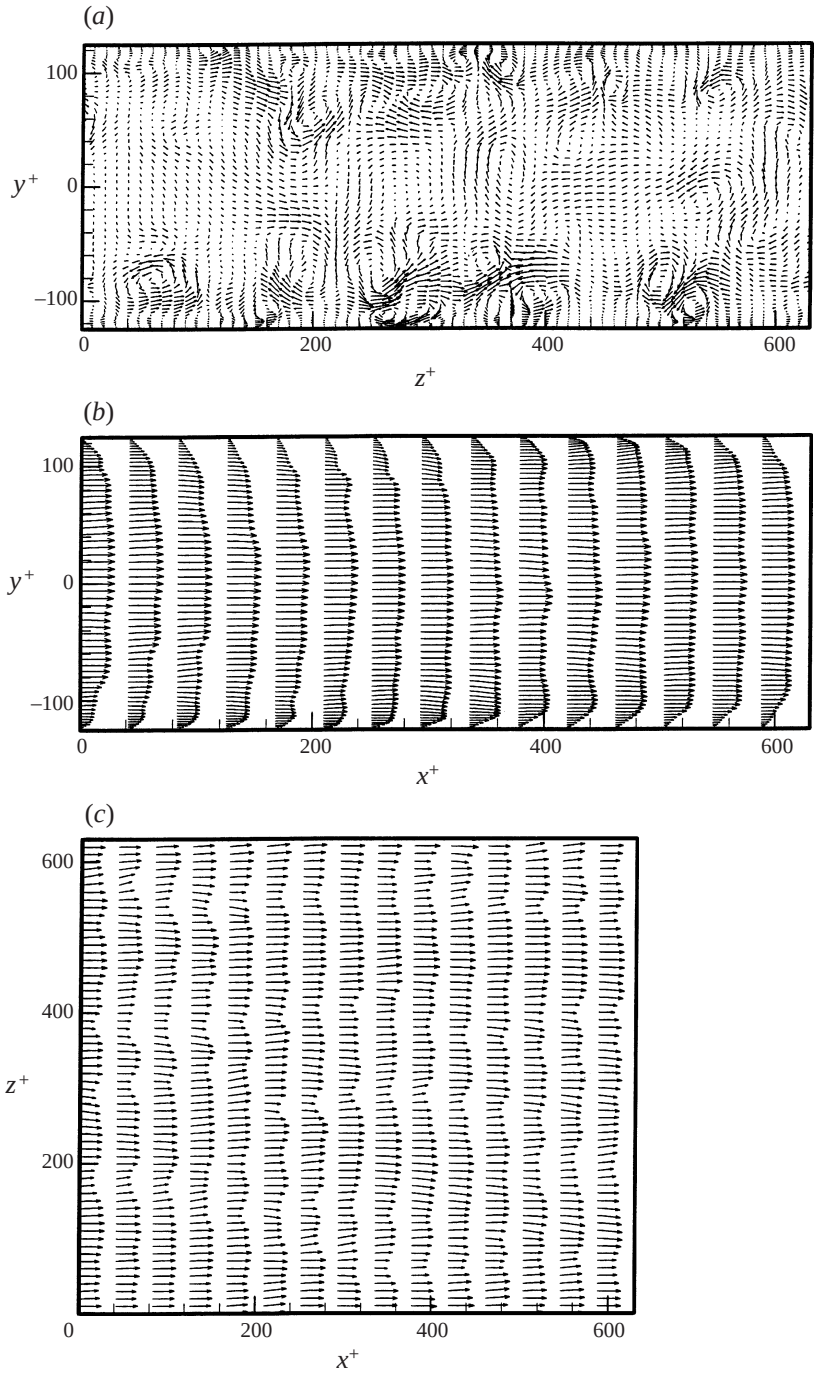

FIGURE 1. Sample velocity plots in (*a*) the (y, z)-plane at $x^+ = 157.5$, (*b*) the (x, y)-plane at $z^+ = 157.5$, (*c*) the (x, z)-plane at $y^+ = 88.4$; $t^+ = 100$.

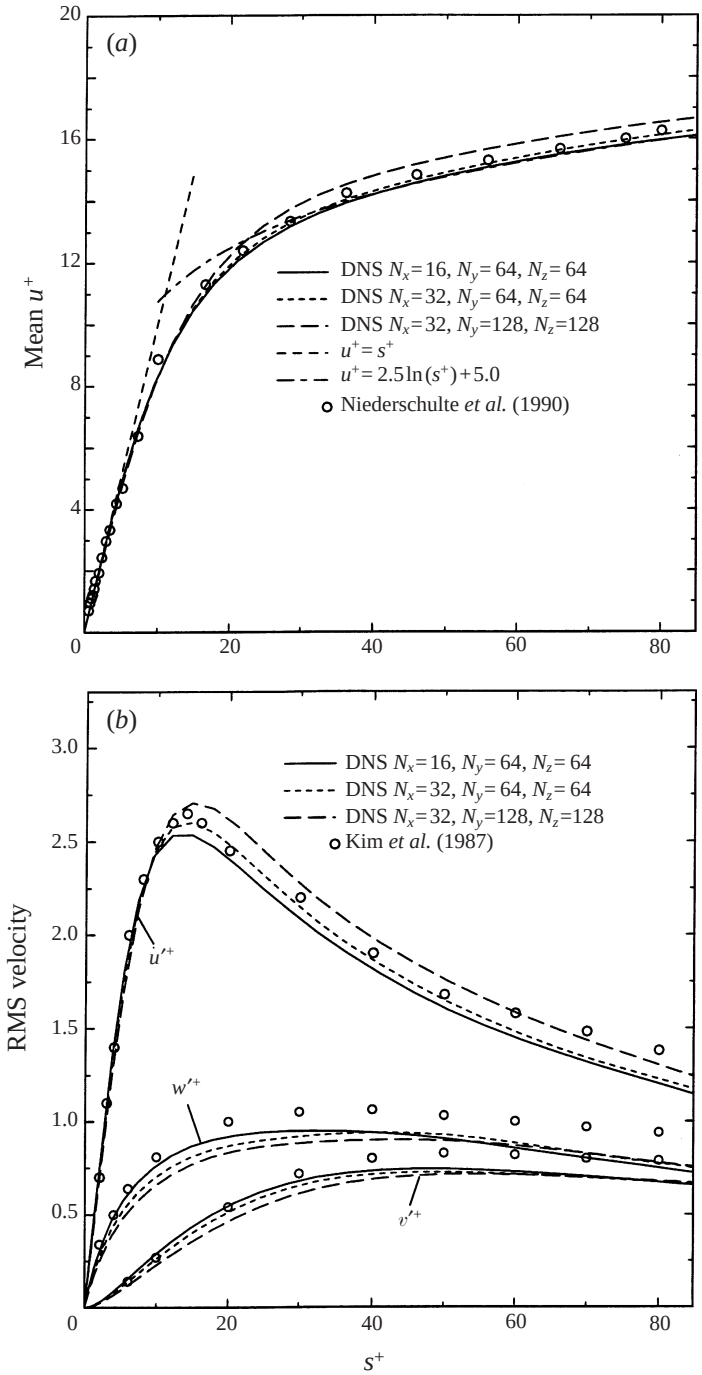

FIGURE 2. (*a*) Mean fluid velocity and (*b*) RMS velocity of DNS with different resolutions.

McLaughlin (1989) showed that the near-wall root-mean-square fluctuation velocities as predicted by the present DNS code are in good agreement with the high-resolution DNS code of Kim, Moin & Moser (1987). Figure 2(*a*) shows the DNS simulation for the present 16 × 64 × 64 grid and the experimental data of

Niederschulte, Adrian & Hanratty (1990) for mean velocity near the wall. Here, s^+ is the non-dimensional distance from the wall. The theoretical linear velocity profile in the viscous sublayer and the logarithmic variations in the inertial sublayer are also shown in this figure for comparison. It is observed that the simulated mean velocity is in good agreement with the data and the classical solutions. The simulated root-mean-square (RMS) fluctuation velocities are shown in figure 2(*b*) and are compared with the earlier high-resolution simulations of Kim *et al.* (1987). In figures 2(*a*) and 2(*b*), the general agreement is reasonable. To test the effect of grid resolution, DNS simulations are repeated for high resolution for grid sizes of $32 \times 64 \times 64$ and $32 \times 128 \times 128$. The resulting mean velocity profiles and turbulence intensities (RMS velocities) are also shown in figures 2(*a*) and 2(*b*), respectively, for comparison. Figure 2 shows that the mean velocity and turbulence intensities do not change appreciably when the grid resolution is increased by a factor of 2 to 8. Therefore, the present DNS with a grid size of $16 \times 64 \times 64$ appears to produce the first-order and second-order turbulence statistics with reasonable accuracy. For the sake of computational economy, this grid is used in the rest of the analyses.

3. Particle equation of motion

The equation of motion of a spherical particle including the nonlinear drag, Brownian, lift and gravitational forces in dimensionless form (in wall units) is given as

$$\frac{\mathrm{d}\boldsymbol{V}^{+p}}{\mathrm{d}t^+} = (1 + 0.15\,Re_p^{0.687})\left(\frac{\boldsymbol{V}^{+f}}{\tau_p^+} - \frac{\boldsymbol{V}^{+p}}{\tau_p^+}\right) + \boldsymbol{n}^+(t^+) + \boldsymbol{g}^+ + \boldsymbol{L}^+ \tag{10}$$

and

$$\frac{\mathrm{d}\boldsymbol{x}^+}{\mathrm{d}t^+} = \boldsymbol{V}^{+p}, \tag{11}$$

where

$$\boldsymbol{x}^+ = \frac{\boldsymbol{x}u^*}{\nu}, \quad \boldsymbol{V}^{+p} = \frac{\boldsymbol{V}^p}{u^*}, \quad \boldsymbol{V}^{+f} = \frac{\boldsymbol{V}^f}{u^*}, \quad t^+ = \frac{tu^{*2}}{\nu}. \tag{12}$$

Here, $\boldsymbol{V}^{+p}$ is the non-dimensional particle velocity, $\boldsymbol{V}^{+f}$ is the non-dimensional instantaneous fluid velocity at the particle location, $\boldsymbol{n}^+(t^+)$ is the non-dimensional Brownian force, $\boldsymbol{g}^+$ is the non-dimensional gravitational force, τ_p^+ is the non-dimensional particle relaxation time, $\boldsymbol{L}^+$ is the non-dimensional lift force, and $Re_p = d|\boldsymbol{V}^f - \boldsymbol{V}^p|/\nu$ is the particle Reynolds number based on the flow–particle slip velocity and the fluid kinematic viscosity. (Note that only the y-component of the lift force is considered in this study.) In (12), u^* is the flow shear velocity.

In (10), the non-dimensional particle relaxation time is give as

$$\tau_p^+ = \tfrac{1}{18} C_c S d^{+2}, \tag{13}$$

where $d^+ = du^*/\nu$ is the dimensionless particle diameter, and $S = \rho^p/\rho^f$ is the particle-to-fluid density ratio. In (13), C_c is the Stokes–Cunningham slip correction factor given as

$$C_c = 1 + \frac{2\lambda}{d}(1.257 + 0.4\mathrm{e}^{-1.1d/2\lambda}), \tag{14}$$

where λ is the molecular mean free path of the gas.

In (10), the non-dimensional Brownian force and the non-dimensional lift force in

the y-direction component are given as

$$n_i^+(t^+) = \frac{6\nu}{\pi\rho^p d^3 u^{*3}} N_i(t^+), \qquad L_y^+ = 3.08 \frac{\mathrm{d}u^+/\mathrm{d}y^+}{Sd^+|\mathrm{d}u^+/\mathrm{d}y^+|^{1/2}}(u^+ - u^{p+}). \tag{15}$$

The spectral intensity of n_i^+ is given by (Ounis *et al.* 1991, 1993)

$$S_{n_i^+ n_j^+}(\omega^+) = \frac{648}{\pi C_c^2} \frac{\delta_{ij}}{S_c S^2 d^{+4}} = \frac{2}{\pi S_c \tau_p^{+2}} \delta_{ij}, \tag{16}$$

where

$$S_c = \frac{\nu}{D} = \frac{3\pi\nu d\mu}{C_c k T} \tag{17}$$

is the Schmidt number, ω^+ is the frequency in wall units, T is the air temperature, μ is the air viscosity, $k = 1.38 \times 10^{-23}\,\mathrm{J\,K^{-1}}$ is the Boltzmann constant, and D is the particle Brownian diffusivity. In (10), the non-dimensional acceleration due to gravity is defined as

$$g_i^+ = \frac{\nu}{u^{*3}} g_i, \tag{18}$$

where g_i are the components of acceleration of gravity.

Ounis & Ahmadi (1989, 1990) showed that the virtual mass, the Faxén correction, Basset history effects, and pressure gradient forces have little effect on the diffusion of small particles considered in this analysis. Hence these forces are not included in (10).

4. Deposition velocity and empirical models

The dimensionless deposition velocity for particles released with a uniform concentration C_0 near a surface is defined as

$$u_d^+ = J/C_0 u^*, \tag{19}$$

where J is the particle mass flux to the wall per unit time. In the computer simulation, the particle deposition velocity may be estimated as

$$u_d^+ = \frac{N_d/t_d^+}{N_0/y_0^+}, \tag{20}$$

where N_0 is the initial number of particles uniformly distributed in a region within a distance of y_0^+ from the wall, and N_d is the number of deposited particles in the time duration t_d^+. In practice, the time duration should be selected in the quasi-equilibrium (stationary) condition when N_d/t_d^+ becomes constant.

In this study, the digital simulation results are compared with the semi-empirical model predictions. A simple empirical equation for the non-dimensional particle deposition velocity is given as

$$u_d^+ = 0.085 S_c^{-2/3} + 4.5 \times 10^{-4} \tau_p^{+2} + \tau_p^+ \hat{\boldsymbol{g}}^+ \cdot \hat{\boldsymbol{j}}, \tag{21}$$

where S_c is the Schmidt number. The first term in (21) is particle deposition due to Brownian motion and eddy diffusion as derived by Cleaver & Yates (1975). The second term is particle deposition induced by eddy diffusion-impaction as suggested by Wood (1981*a*). The last term in (21) accounts for the gravitational sedimentation on the lower wall of horizontal ducts. Note that (21) neglects the variation of deposition rate with the direction of gravity when the gravity is along the flow direction.

Fan & Ahmadi (1993) developed an empirical equation to evaluate the deposition

rate for vertical ducts including the effect of gravity direction and surface roughness, which is given as

$$u_d^+ = \begin{cases} 0.084Sc^{-2/3} + \dfrac{1}{2}\left[\dfrac{\left(0.64k^+ + \frac{1}{2}d^+\right)^2 + \dfrac{\tau_p^{+2}g^+L_1^+}{0.01085(1+\tau_p^{+2}L_1^+)}}{3.42 + (\tau_p^{+2}g^+L_1^+)/(0.01085(1+\tau_p^{+2}L_1^+))}\right]^{1/(1+\tau_p^{+2}L_1^+)} \\ \quad \times \left[1 + 8\mathrm{e}^{-(\tau_p^+-10)^2/32}\right]\dfrac{0.037}{1-\tau_p^{+2}L_1^+(1+(g^+/0.037))} & \text{if } u_d^+ < 0.14 \\ 0.14 & \text{otherwise.} \end{cases} \tag{22}$$

Here, $L_1^+ = 3.08/(Sd^+)$, and k^+ is the surface roughness (which is zero in this study). For a horizontal channel, $g^+ = 0$ in (22) and the gravitational sedimentation velocity $\tau^+ g^+$ must be added. Equation (22) is used in the following section for comparison with the DNS results for particle deposition rate.

5. Simulation results

In this section, results concerning transport and deposition of small aerosol particles from turbulent air streams in vertical and horizontal ducts are presented. In the simulation, a temperature of $T = 298\,\mathrm{K}$, a kinematic viscosity of $\nu = 1.5\times10^{-5}\,\mathrm{m^2\,s^{-1}}$, and a density of $\rho^f = 1.12\,\mathrm{kg\,m^{-3}}$ for air are assumed. The flow Reynolds number, Re^*, based on the shear velocity, u^*, and half-channel width is 125, while Re based on the hydraulic diameter and the centreline velocity is about 8000. The density ratio and shear velocity are varied, and their effects on particle deposition rates in vertical and horizontal ducts are studied. An ensemble of 8192 particles for each diameter is used for particle trajectory statistics and deposition velocity analyses.

5.1. *Vertical duct*

Particle deposition from turbulent flow in a vertical channel is treated first. The results for the case when the flow is in a downward direction are compared with those in the absence of the gravitational effect. (The latter case corresponds to the particle deposition on the sidewall of a horizontal duct.)

In the first set of simulations, particles are initially distributed with a uniform concentration between 1 and 30 wall units; and particle trajectories are evaluated for a duration of 100 wall units of time. The streamwise direction is along the x-coordinate, and $y^+ = \pm125$ are the locations of the sidewalls. Figure 3 shows sample variations of the number of deposited particles versus time for different diameters under the condition that shear velocity is $0.2\,\mathrm{m\,s^{-1}}$, density ratio is 1000 and gravity is in the flow direction. It is observed that the number of deposited particles increases with particle diameter in the size range shown in this figure. The number of deposited particles reaches its equilibrium limit after 30 to 50 wall units of time, and then reduces due to the depletion of particle and/or their dispersion away from the wall.

Figures 4(a) and 4(b), respectively, show time variations of various forces acting in the y-direction near the wall on randomly selected particles with diameters of $15\,\mu\mathrm{m}$ and $0.1\,\mu\mathrm{m}$ for a shear velocity of $0.3\,\mathrm{m\,s^{-1}}$ and a density ratio of 1000. Gravity is in the streamwise direction, and the forces are recorded for duration of 100 wall units of time. For the $15\,\mu\mathrm{m}$ particles, figure 4(a) shows that the drag is the dominating

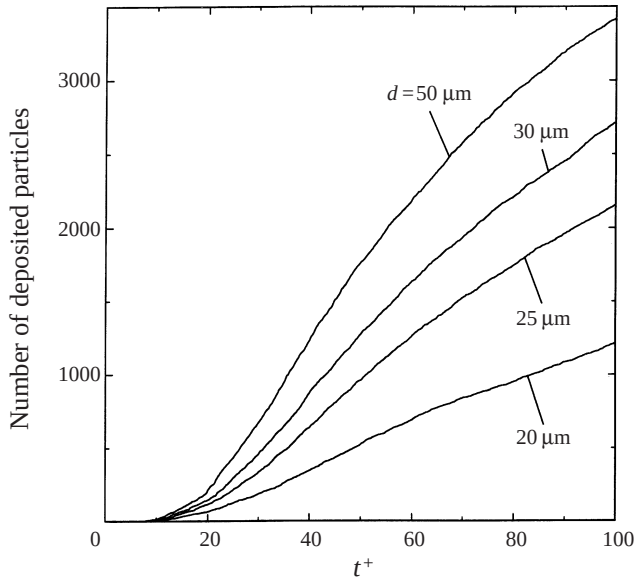

FIGURE 3. Variations of the number of deposited particles versus time for different particle diameters.

force which is roughly balanced by the inertia force. The lift force is about 5% to 10% of the drag force. The Brownian force is negligibly small for these relatively large particles. The Brownian force, however, increases rapidly when the diameter of particles decreases to submicrometer range. Figure 4(*b*) shows that the Brownian, the drag and the inertia forces are of the same order, and the lift force is quite small for a 0.1 μm particle. Therefore, for particles smaller than 0.1 μm, the Brownian motion plays an important role.

Sample time variations of particle Reynolds number for three randomly selected particles with diameters of 1, 15 and 50 μm for the case of downward airflow with a shear velocity of 0.3 m s^{-1} are shown in figure 4(*c*). It is observed that the particle Reynolds number, Re_p, for the 1 μm particle is less than 10^{-3}, and Re_p for the 15 μm particle is less than 0.7; therefore, the nonlinear correction factor for the drag force in (10) is negligible for a particle diameter less than 15 μm. Re_p for 50 μm particles oscillates with time and its magnitude reaches to about 3. Thus, the nonlinear correction to the drag is important for large particles.

To evaluate the effect of the nonlinear correction for the drag force on the deposition velocities, several simulations are performed and the cases with or without nonlinear correction are analysed. The corresponding results, figure 4(*d*), show that the effect of the nonlinear correction on particle deposition velocity is negligible even though particle Reynolds number could sometimes become large for large particles. Thus, the simulated particle deposition velocity is not sensitive to the variation of nonlinear drag coefficient for particle size less than 50 μm and shear velocities less than 0.3 m s^{-1}. Nevertheless, the nonlinear drag was included in simulation analyses for completeness.

The streaky structure of the viscous sublayer of turbulent near-wall flows was summarized by Hinze (1975) and Smith & Schwartz (1983). In the earlier works of Ounis *et al.* (1993) and Soltani & Ahmadi (1995), it was shown that the turbulence near-wall coherent eddies play a dominant role in particle deposition and resuspension processes. To study the effect of coherent eddy structures on particle deposition in

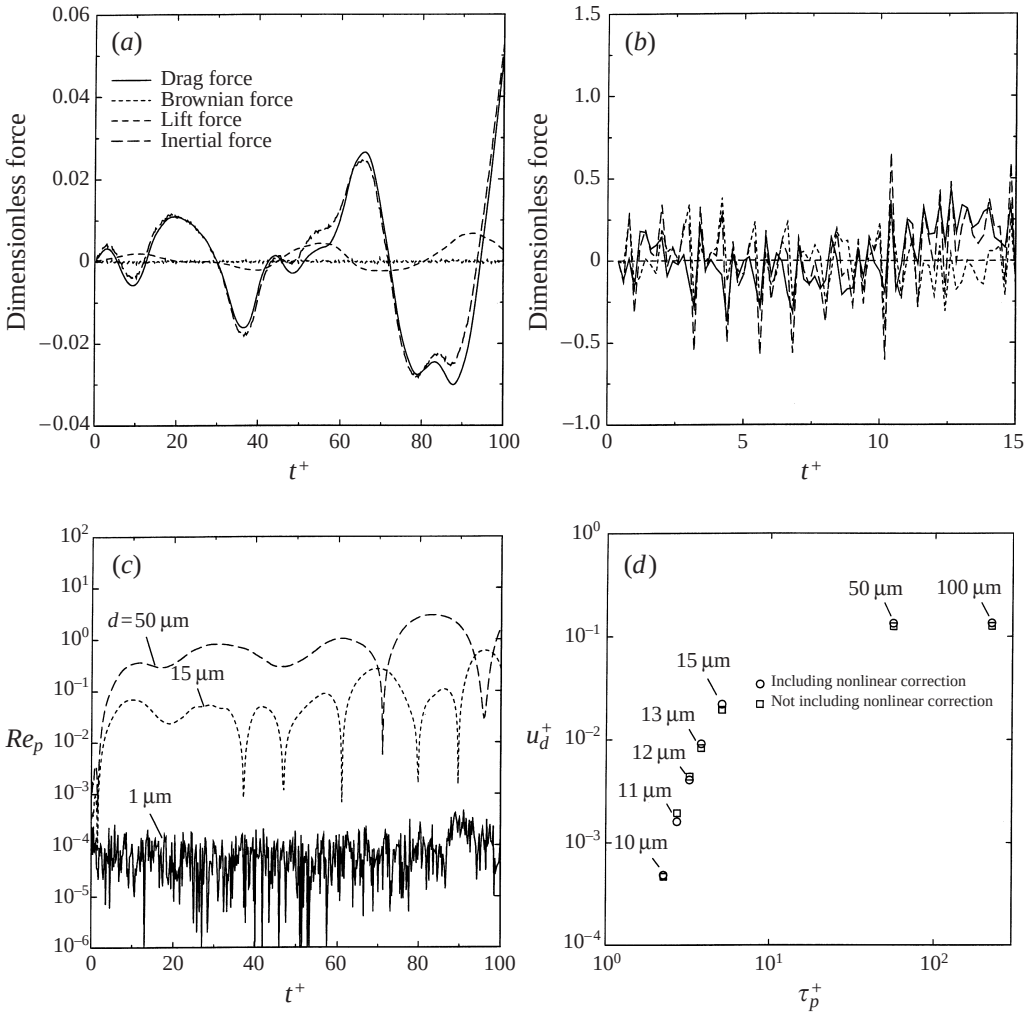

FIGURE 4. (a, b) Time variations of various forces for (a) a 15 μm particle and (b) a 0.1 μm particle, (c) Sample time variations of particle Reynolds number, $u^* = 0.3\,\mathrm{m\,s^{-1}}$, gravity in the flow direction (d) Effect of nonlinear correction on deposition velocity, $u^* = 0.3\,\mathrm{m\,s^{-1}}$, $S = 1000$, gravity in the flow direction.

the presence of gravitational effects, a simulation is performed with initial particle positions being uniformly distributed in a region with a width of 12 wall units from the upper wall which covers the peak fluctuation-energy generation region. Here, gravity is assumed to be in the streamwise direction, and particle diameters of 0.01, 15, 25, and 50 μm are studied. Figures 5(a) and 5(b), respectively, show the initial locations of the deposited 0.01 and 15 μm particles in a time duration of 0–100 wall units. It is observed that the initial locations of deposited 0.01 μm particles are randomly distributed. This is because, for submicrometre particles, the Brownian diffusion strongly affects the deposition process so that the effect of turbulence coherent eddies is smeared. Figure 5(b) shows that the initial locations of deposited 15 μm particles in the (x, z)-plane are concentrated in certain bands, which are about 100 wall units apart. Similar results for 25 and 50 μm particles that are deposited in the time duration 50–100 wall units are displayed in figures 5(c) and 5(d). An examination

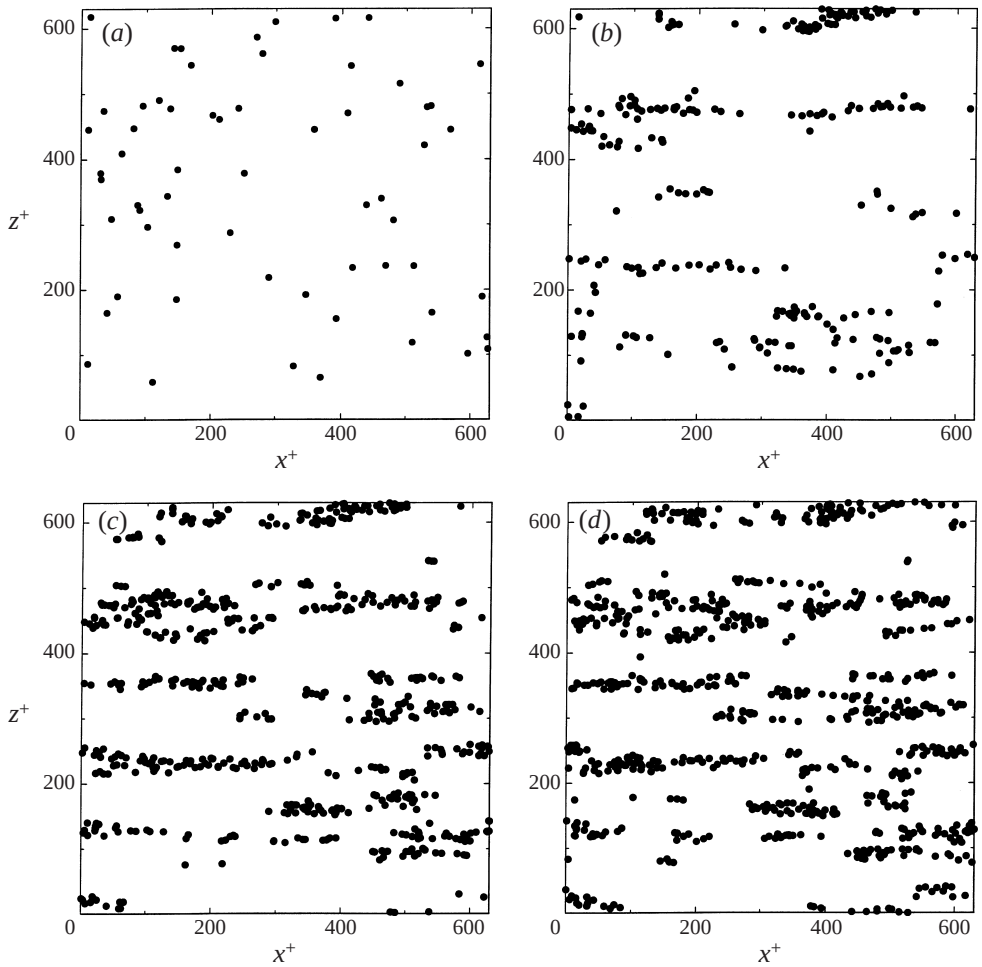

FIGURE 5. Distribution of the initial locations of deposited particles in the (x, z)-plane: (*a*) $d = 0.01\,\mu$m, (*b*) $0.15\,\mu$m, (*c*) $25\,\mu$m, (*d*) $50\,\mu$m.

of these figures shows that the initial locations of these deposited particles are also scattered around the same lines that are at a distance of about 100 wall units from each other. We have repeated these simulations with the particles being distributed initially in a wider region of 30 wall units from the wall. For the $15\,\mu$m particles, the results for the initial locations of the deposited particles remain essentially unchanged. For larger particles, however, the lines become cluttered, but the general feature does not change. (These additional results, however, are not shown here due to space limitation.)

Figures 6(*a*) and 6(*b*), respectively, show contour plots of short-time mean fluid velocities in the streamwise direction, u^+, and normal to the wall, v^+, in the (y, z)-plane near the upper wall. The short-time mean fluid velocities are obtained by spatial averaging over a distance of 630 wall units in the streamwise direction for a time duration of 100 wall units. Figure 6(*a*) shows that the mean streamwise velocity has a roughly periodic variation in the spanwise direction with the distance between adjacent high-speed (or low-speed) regions being about 100 wall units. Similar results for the v^+-velocity in figure 6(*b*) show alternating streams toward and away from

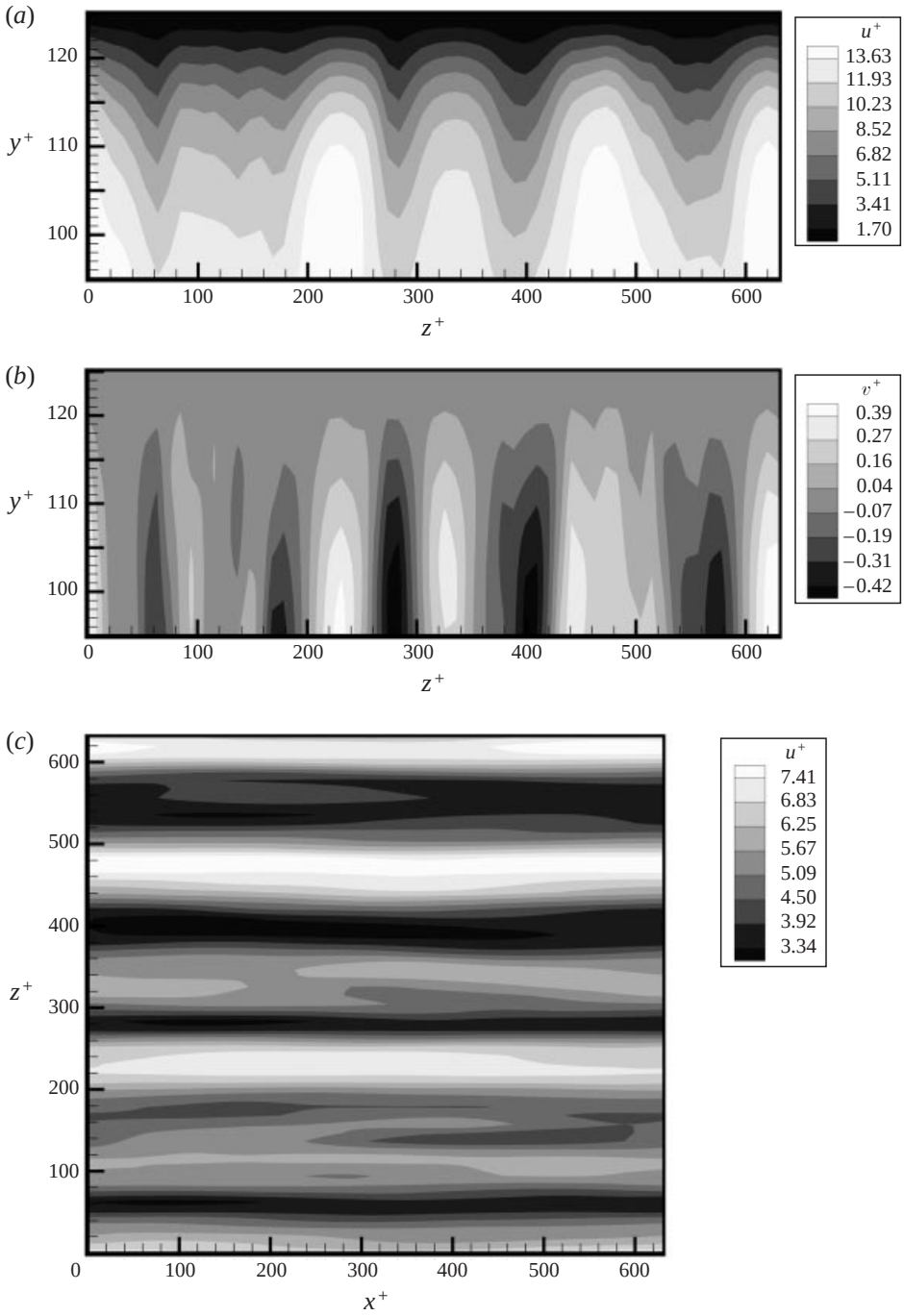

FIGURE 6. Contour plots of (*a*) mean u^+ in the (y, z)-plane, (*b*) mean v^+ in the (y, z)-plane, (*c*) mean u^+ in the (x, z)-plane.

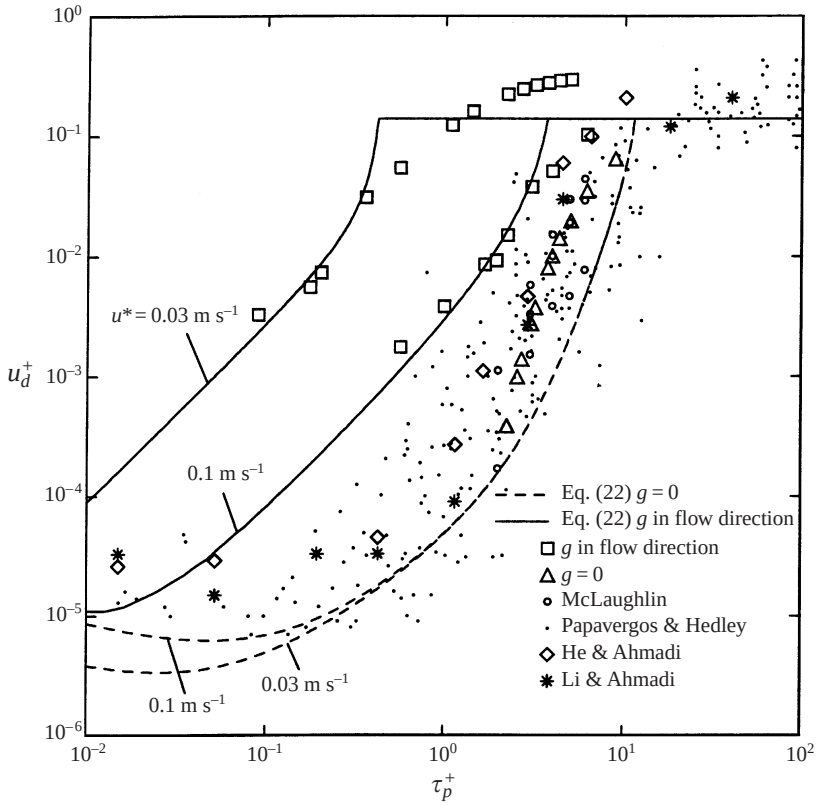

FIGURE 7. Variations of deposition velocity with particle relaxation time for different shear velocities; $S = 1000$.

the upper wall. Comparing figures 6(*a*) and 6(*b*) it is observed that the locations of high-speed axial streams roughly correspond to the regions where the flow moves toward the wall, and the low-speed axial streams, on the average, coincide with the regions where the flow moves away from the wall.

Figure 6(*c*) shows the contour plot of the short-time mean streamwise velocity, u^+, in the (x, y)-plane, where spatial averaging is performed over the region within 12 wall units from the upper wall. Alternating bands of high and low velocities can be clearly seen from this figure. The spacing between the high-speed (low-speed) bands is again about 100 wall units. Comparing figure 6 with figure 5(*c*) shows that the initial locations of deposited particles coincide with the high-speed axial stream regions, which are also the regions where strong streams toward the wall are formed. The formulation of these bands is clearly due to the near-wall coherent eddies. That is, particles which are in the downflow regions (toward the wall) of the counter-rotating streamwise vorticies are carried toward the wall and are deposited. Thus, the near-wall streamwise eddies play an important role in the particle deposition process even in the presence of gravity (in the streamwise direction). This observation is consistent with that of Ounis *et al.* (1993). Earlier, Soltani & Ahmadi (1995) showed that the near-wall flow structures strongly affect the particle removal process, as well.

To evaluate the effect of gravity and its direction on the particle deposition rate in vertical turbulent duct flows, several computer simulations were performed. The

Shear velocity	Vertical duct	Horizontal duct
0.03 ($m\,s^{-1}$)	148	—
0.1 ($m\,s^{-1}$)	14	201
0.2 ($m\,s^{-1}$)	0.45	—
0.3 ($m\,s^{-1}$)	0.10	6.1

TABLE 1. Estimated values of Δu_d^+ for different shear velocities.

effect of variations in density ratio and shear velocity was also studied. For a vertical duct with shear velocities of 0.03 and 0.1 $m\,s^{-1}$, and a density ratio of 1000, figure 7 shows the variation of the simulated non-dimensional deposition velocity, u_d^+, versus non-dimensional particle relaxation time. This figure shows the direct numerical simulation results for two cases: gravity in the flow direction (i.e. downward flow in the vertical duct), and the gravitational effect absent. For $g = 0$, the DNS simulation results for $u^* = 0.03$ and 0.1 $m\,s^{-1}$ are also shown in this figure. The numerical results of McLaughlin (1989) and the experimental data collected by Papavergos & Hedley (1984) and the simulation results of He & Ahmadi (1999) and Li & Ahmadi (1993) are also reproduced in this figure for comparison. The deposition velocities predicted by the sublayer-based empirical equation given by (22) are also shown. The solid and dashed lines are, respectively, for gravity in the flow direction and the absence of gravity. As expected, the deposition velocity increases sharply with τ_p^+ and reaches a saturation level.

Figure 7 shows that the particle deposition velocity in a vertical channel is significantly enhanced when the gravity is in the flow direction. In particular, for $u^* = 0.03\,m\,s^{-1}$, the deposition rate for a downward gas flow in a vertical duct is about two orders of magnitude higher than that on the sidewalls in a horizontal duct. According to Fan & Ahmadi (1993), when gravity is in the flow direction, the shear-induced lift force is toward the wall (since the heavy particles move faster than the fluid). Therefore the deposition rate increases for downward flows in vertical ducts. On the other hand, when gravity is in the opposite direction (i.e. upward flow), the lift force tends to move the particles away from the wall, and the deposition velocity decreases. For $u^* = 0.03$ and 0.1 $m\,s^{-1}$, figure 7 shows that the DNS results are in good agreement with the results predicted by the model of Fan & Ahmadi (1993) as given by (22) for both gravity in the flow direction and in the absence of gravity. The earlier simulation results of McLaughlin (1989), Li & Ahmadi (1993) and He & Ahmadi (1999) in the absence of gravity are in general agreement with the present DNS predictions. The DNS results for $u^* = 0.1\,m\,s^{-1}$ and downward flows are at the upper end of the experimental data, while those for $u^* = 0.03\,m\,s^{-1}$ are much higher. The reason is that most experimental studies were performed at much higher velocities, and the depositions were measured on the sidewalls of a horizontal duct for which the effect of gravity is negligible.

The DNS results for particle deposition in ducts with shear velocities of 0.2 and 0.3 $m\,s^{-1}$ are shown in figures 8(*a*) and 8(*b*), respectively. Here, density ratios of $S = 1000$ and $S = 2000$ are considered and cases in which the flow is upward or downward are simulated. Figure 8 shows that the particle deposition velocity is only slightly enhanced when gravity is in the direction of flow when compared with the case in which gravity is opposing the flow. That is, for high-speed flows, the changes in the deposition velocity due to the effect of gravity direction are much smaller than those

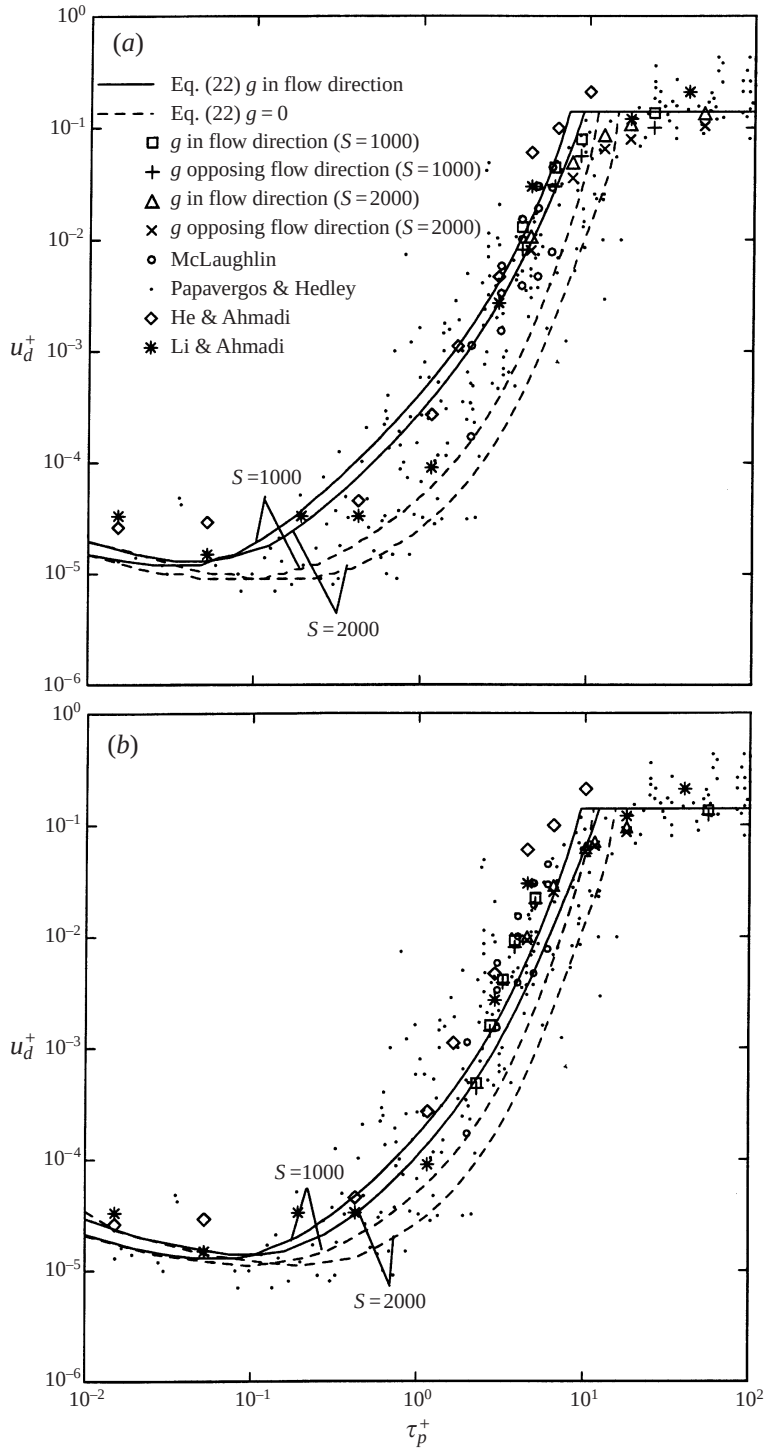

FIGURE 8. Variations of deposition velocity with particle relaxation time for different density ratios. (*a*) $u^* = 0.2\,\mathrm{m\,s^{-1}}$, (*b*) $u^* = 0.3\,\mathrm{m\,s^{-1}}$.

for flows with low shear velocities. While the direct simulation results are in general agreement with equation (22), the differences between the deposition velocities for upward and downward flows are smaller than those predicted by the empirical model. Figure 8 shows that the non-dimensional deposition for $0.01 \leqslant \tau_p^+ \leqslant 10$ decreases when the particle-to-fluid density ratio, S, increases. The effect of variation of S on the deposition velocity, however, is small. Figure 8 also shows that the DNS and the empirical model predictions for shear velocities of 0.2 and $0.3\,\mathrm{m\,s^{-1}}$ and density ratios of 1000 and 2000 are in the range of variation of the experimental data.

To further understand the effect of the direction of gravity on the particle deposition rate or different shear velocities, the mean relative change of deposition velocity defined as

$$\Delta u_d^+ = \frac{1}{N}\sum_{i=1}^{N}\left(\frac{u_g^{i+} - u_{g=0}^{i+}}{u_{g=0}^{i+}}\right) \tag{23}$$

is evaluated, where u_g^{i+} is the deposition velocity when the gravity is in the flow direction, $u_{g=0}^{i}$ is the deposition velocity in the absence of gravitation effects, and N is the total number of simulation data points used. Table 1 shows the values of Δu_d^+ for different shear velocities as obtained from the present DNS results. Clearly, the magnitude of the shear velocity strongly affects the contribution of the gravity direction to the deposition rate. When the shear velocity is smaller than $0.1\,\mathrm{m\,s^{-1}}$, the effect of gravity and its direction on the particle deposition rate becomes truly significant. As noted before, when the shear velocity is small, g^+ becomes large and the particle–fluid slip velocity increases; thus, the shear-induced lift force becomes quite large and the effect of gravity direction becomes very important. At high shear velocities, g^+ becomes small and table 1 shows that the gravity-enhanced deposition rate is reduced.

For shear velocities of 0.03 and $0.1\,\mathrm{m\,s^{-1}}$, figure 9 shows the empirical model predictions for variation of deposition velocity for different particle-to-fluid density ratios. The simulation results are also shown in this figure for comparison, and are found to be in good agreement with the empirical model predictions for different particle-to-fluid ratios. It is observed that the effect of density ratio on particle deposition rate is comparatively small. For a given particle relaxation time, when the density ratio is doubled, the deposition velocity decreases by less than 30%. In the absence of gravity, figure 9 shows that the deposition rate for a fixed density ratio is not affected by variation in the shear velocities for particles with $\tau_p^+ > 1$. This is because, for large particles, the Brownian diffusion is negligible, and the turbulence eddy diffusion-impaction is dominant. For particles with $\tau_p^+ < 0.1$, however, the variation of u^* alters u_d^+, since the Brownian diffusion (which is independent of u^*) contributes to the deposition velocity.

5.2. *Plane source*

In the second set of simulations, dispersion and deposition from plane sources of particles that are initially released at a distance of 5 wall units from the bottom wall are studied. Here, an ensemble of 8192 particles with $d = 50\,\mu\mathrm{m}$, a density ratio of S=1000, and a shear velocity of $0.1\,\mathrm{m\,s^{-1}}$ is used. At every time step, the mean, the standard deviation, and the absolute maximum and minimum of particle positions are computed. Figures 10(*a*) and 10(*b*), respectively, show the results for the cases in which gravity is along the flow direction, and gravitational effects are neglected. When gravity is along the flow, figure 10(*a*) shows that the mean particle path is a straight line roughly parallel to the wall. In the absence of gravity, however, the

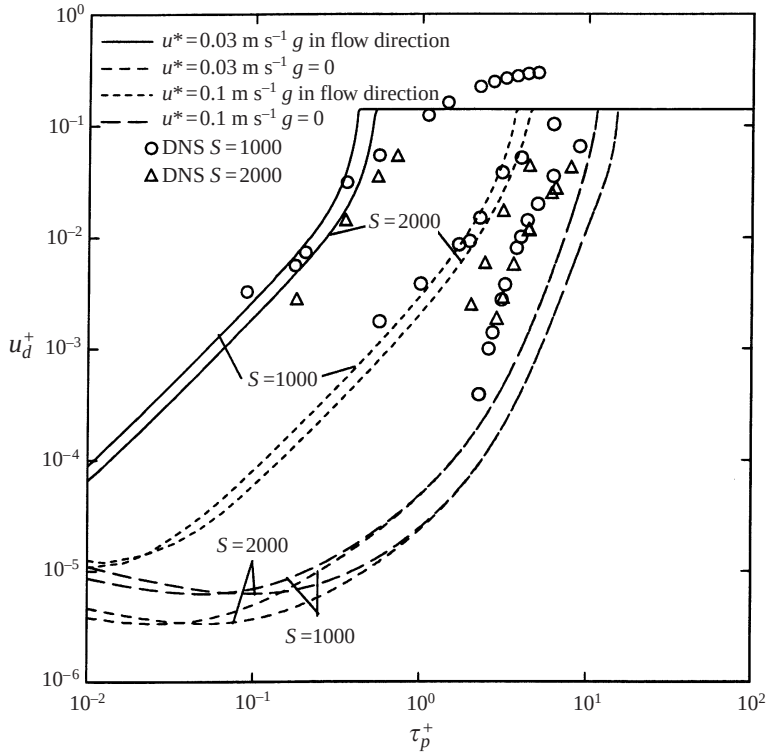

FIGURE 9. Effects of density ratio on deposition velocity at various shear velocities.

mean particle path shown in figure 10(*b*) moves away from the wall. That is, when gravity is in the flow direction, the particles stay near the wall; while in the absence of gravity, the particles move away from the wall, and the deposition rate decreases. It is also noticed that the absolute maximum particle positions in the presence or absence of gravity are quite similar. This is because the lift force decreases rapidly with the distance from the wall, and the effect of lift-induced migration decreases. Therefore, the effect of gravity direction far from the wall becomes very small.

5.3. *Mean force*

To illustrate the effect of gravity direction on the particle deposition process, additional simulations for shear velocities of 0.1, 0.2 and 0.3 m s^{-1} and S=1000 are performed. An ensemble of 8192 particles with $\tau_p^+ = 5$ is used in simulations, and particles are initially randomly distributed in the region within 30 wall units from the lower wall. (Note that the corresponding particle diameters are 45, 22.5 and 15 μm with sedimentation velocities, $\tau^+ g^+$, being 0.735, 0.092 and 0.027 in wall units.) At every time step, the ensemble averages of the drag, the lift and the absolute values of Brownian forces in the y-direction acting on particles that are moving in the region within 12 wall units from the bottom wall are computed. (Positive sign denotes that the direction is away from the lower wall.) The mean particle–fluid slip velocity in the streamwise direction at every time step is evaluated using $(1/N_p)\sum_{i=1}^{N_p}(u_i^{p+} - u_i^{f+})$, where N_p is the total number of particles, u_i^{p+} is the particle velocity and u_i^{f+} is the fluid velocity at the particle location. Here, streamwise direction is considered positive. The simulation results for the time duration of 20 to 100 wall units are shown in

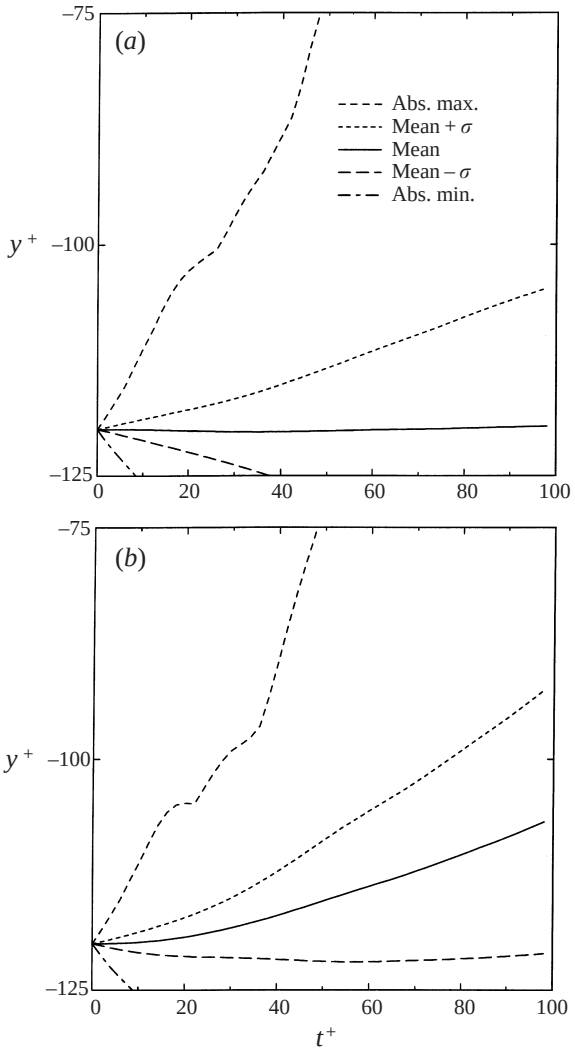

FIGURE 10. Particle trajectory statistics for $d = 50\,\mu\text{m}$, $u^* = 0.1\,\text{m}\,\text{s}^{-1}$ and (*a*) g in the flow direction and (*b*) $g = 0$.

figures 11 and 12 (i.e. the time after the startup to 20 wall units is omitted to eliminate the effect of initial conditions).

Figure 11 shows the variation of the mean slip velocity versus time for particles with $\tau_p^+ = 5.0$ at various shear velocities (particle sizes). It is observed that the slip velocity for downward flows is larger than that for upward flows, and the difference of mean slip velocities due to different flow directions increases as shear velocity decreases (particle size increases). This further shows that the effect of gravity direction is significant for low shear velocities and large particles. For $u^* = 0.1\,\text{m}\,\text{s}^{-1}$ ($d = 45\,\mu\text{m}$), mean slip velocity is positive for downward flows and negative for upward flows. Thus, the lift force will act towards the wall for downward flows and away from the wall for upward flows. For shear velocities greater than $0.2\,\text{m}\,\text{s}^{-1}$, the change of gravity direction has a small effect on the slip velocity, and the particles usually move faster than the fluid in the streamwise direction near the wall. Thus, the particles

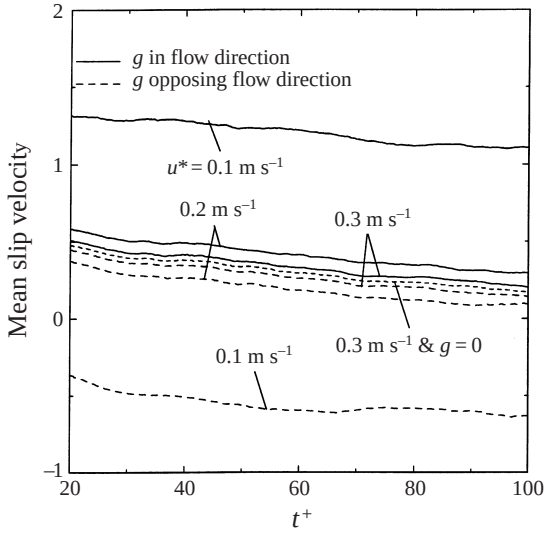

FIGURE 11. Velocity deviation between particle and fluid for various shear velocities; $\tau_p^+ = 5$, $S = 1000$.

will experience a lift force towards the wall for both downward and upward flows. For $u^* = 0.3\,\mathrm{m\,s^{-1}}$, figure 11 shows that for flows in the downward and upward directions, as well as in the absence of gravity, particles move faster than the fluid in the streamwise direction and the effect of gravity is small. Figure 11 also suggests that the particles are being transported towards the wall perhaps by the down sweep motion of the coherent near-wall eddies, and therefore they carry larger streamwise velocity compared to that of the surrounding fluid.

Figure 11 also shows that the difference of mean slip velocities for downward and upward flows for u^* of 0.1, 0.2 and $0.3\,\mathrm{m\,s^{-1}}$ are, respectively about 1.7, 0.2 and 0.05 in wall units. These values are approximately twice the gravitational sedimentation velocities of 0.735, 0.092 and 0.027 for these respective cases. This observation suggests that the gravitation sedimentation velocity is linearly superposed on the mean particle velocities in turbulent duct flows. The results for $\tau_p^+ = 5.0$ show that, for shear velocities of the order of $0.1\,\mathrm{m\,s^{-1}}$ or smaller, the effect of gravity direction becomes significant, and the slip velocity switches sign and becomes negative for upward flows (indicating that particles move slower than the surrounding fluid in the streamwise direction near the wall). For large shear velocities, however, the effect of gravity becomes negligible.

Figure 12 shows variations of different mean forces acting in the y-direction on particles with $\tau_p^+ = 5.0$ versus time for different shear velocities. Figure 12(a) indicates that for $u^* = 0.3\,\mathrm{m\,s^{-1}}$ for particles with $\tau_p^+ = 5$ ($d = 15\,\mu\mathrm{m}$, $\tau^+ g^+ = 0.027$), the mean lift force is toward the wall, the mean drag is away from the wall, and the Brownian effect is negligible. The magnitudes of the mean drag (in the y-direction) and the mean lift force change slightly as the direction of gravity is changed. The positive drag force indicates that there is a trend of particle migration toward the wall. As noted before, the effect of gravity at high shear velocities is relatively small.

For $u^* = 0.1\,\mathrm{m\,s^{-1}}$, figure 12($b$) shows that the mean lift force changes direction due to the effect of gravity. For upward flows, the mean lift force tends to move particle away from the wall, because the particles generally move slower than the fluid in the streamwise direction near wall. For downward flows, the mean lift force is negative

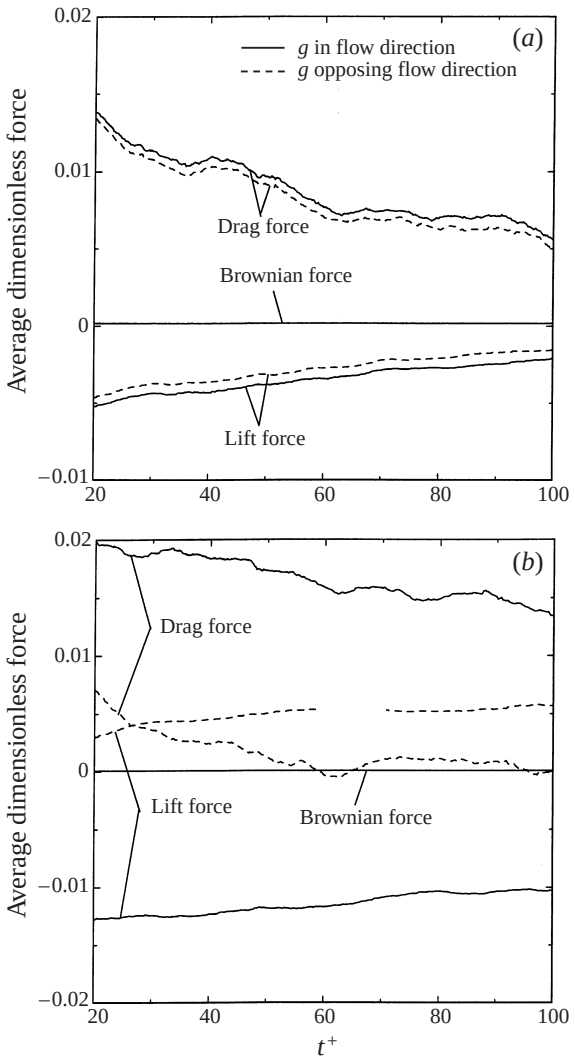

FIGURE 12. Time varations of averaged forces for particles with $\tau_p^+ = 50$: (*a*) $u^* = 0.3\,\mathrm{m\,s^{-1}}$, (*b*) $u^* = 0.1\,\mathrm{m\,s^{-1}}$.

and large, thus increasing the particle deposition velocity. Figure 12(*b*) also shows that for downward flows, the drag is positive providing resistance to particles moving toward the wall. For upward flows, the mean drag force is generally positive but small, and even occasionally becomes negative for a brief time duration. This implies that the particles are moving very slowly toward the wall and sometimes move away from the wall, perhaps by the action of the lift force.

5.4. *Horizontal duct*

Simulation results concerning particle deposition for turbulent flows in a horizontal duct are described in this section. Figure 13 shows the simulated deposition velocity versus particle relaxation time when gravity is perpendicular to the wall for shear velocities of 0.1 and $0.3\,\mathrm{m\,s^{-1}}$ and a particle-to-fluid density ratio of 1000. Simulation results for $g^+ = 0$ (and $u^* = 0.1$ and $0.3\,\mathrm{m\,s^{-1}}$), the predictions of (22), the experimental

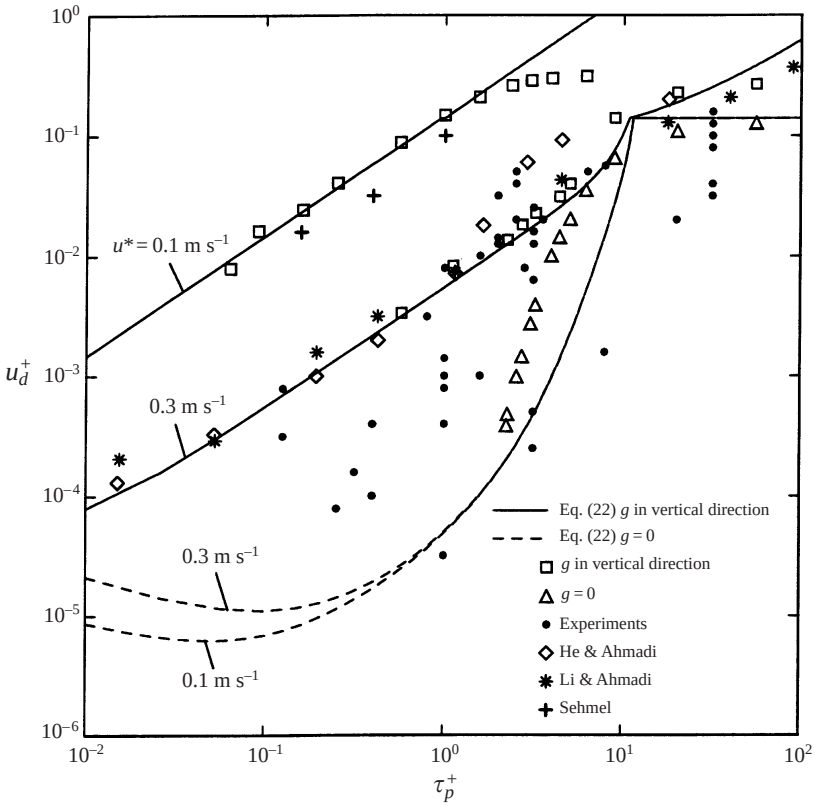

FIGURE 13. Variations of deposition velocity with particle relaxation time for horizontal ducts; $S = 100$.

data from Anderson & Russell (1970), Montgomery (1969), and Sehmel (1973), and the simulation results of He & Ahmadi (1999) and Li & Ahmadi (1993) (for $u^* = 0.3\,\mathrm{m\,s^{-1}}$) for horizontal ducts are also shown in this figure for comparison. It is observed that the non-dimensional deposition velocity increases sharply due to the gravitational sedimentation effects. The amount of increase is also a strong function of magnitude of shear velocity, with u_d^+ increasing rapidly as u^* becomes small. The experimental data show considerable scatter, which is consistent with the sensitive with dependence of u_d^+ on u^*. The simulation results are also in close agreement with the empirical model predictions and earlier simulation results by Li & Ahmadi (1993) and He & Ahmadi (1999) for $u^* = 0.3\,\mathrm{m\,s^{-1}}$. The DNS results for $u^* = 0.1\,\mathrm{m\,s^{-1}}$ are comparable with the experimental data collected by Sehmel for $u^* = 0.114\,\mathrm{m\,s^{-1}}$.

The mean relative change of deposition velocity for the horizontal channel as computed from (23) is also shown in table 1. As is expected, Δu_d^+ for horizontal ducts is very large and much higher than the corresponding values for the downflow condition in a vertical channel. Figure 13 and table 1 also show that for horizontal ducts, the non-dimensional deposition velocity varies significantly with the magnitude of shear velocity (certainly more than that found for vertical channels).

To study the effect of density ratio on the deposition rate in a horizontal channel, the DNS results and the predictions of (22) for shear velocities of 0.3 and $0.1\,\mathrm{m\,s^{-1}}$ and density ratios of 1000 and 2000 are shown in figure 14. The DNS results are seen to be in good agreement with the empirical model predictions. It is observed

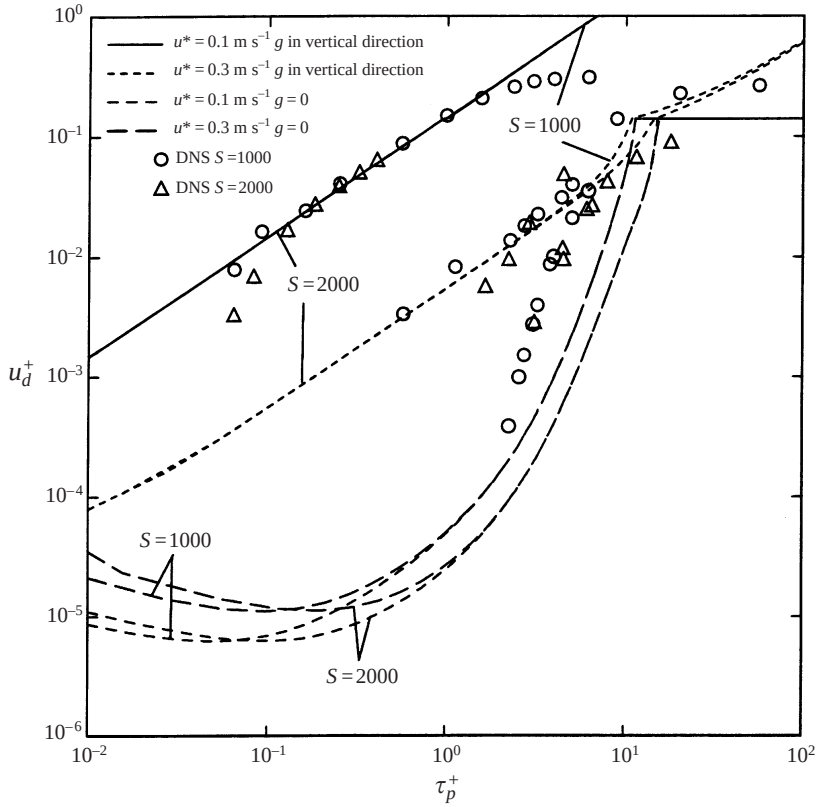

FIGURE 14. Effects of density ratio on deposition velocity at various shear velocities in a horizontal duct.

that when the gravity is perpendicular to the flow direction, the effect of density ratio on non-dimensional deposition velocity is negligible. This is because the gravitational sedimentation velocity $\tau^+ g^+$ makes a dominant contribution to the deposition rate and overwhelms the other density-ratio-dependent effects. Figures 15(*a*) and 15(*b*), respectively show the initial locations of the deposited 15 and 25 μm particles in horizontal ducts. The initial condition is the same as described in the previous section. Figure 15 shows that the initial locations of deposited particles are almost uniformly distributed; thus, the effect of turbulent coherent eddies smears. This is because gravitational sedimentation is the dominant mechanism for particle deposition in horizontal ducts.

5.5. *Plane source*

The dispersion of particles in a horizontal channel in the presence and absence of gravity is studied in this section. An ensemble of 8192 particles with $d = 30\,\mu\text{m}$ is released at a distance of 5 wall units from the bottom wall and the particles' subsequent motions are evaluated. Here, a shear velocity of $0.3\,\text{m}\,\text{s}^{-1}$ and a density ratio of $S = 1000$ are assumed. The mean, the standard deviation, and the absolute maximum and minimum of the particle positions are computed and the results are plotted in figures 16(*a*) and 16(*b*). Figure 16(*a*) shows that, when gravity is toward the wall, the particle trajectory statistics are highly skewed toward the bottom wall. After about 30 wall units of time, the particle mean path practically reaches the lower wall.

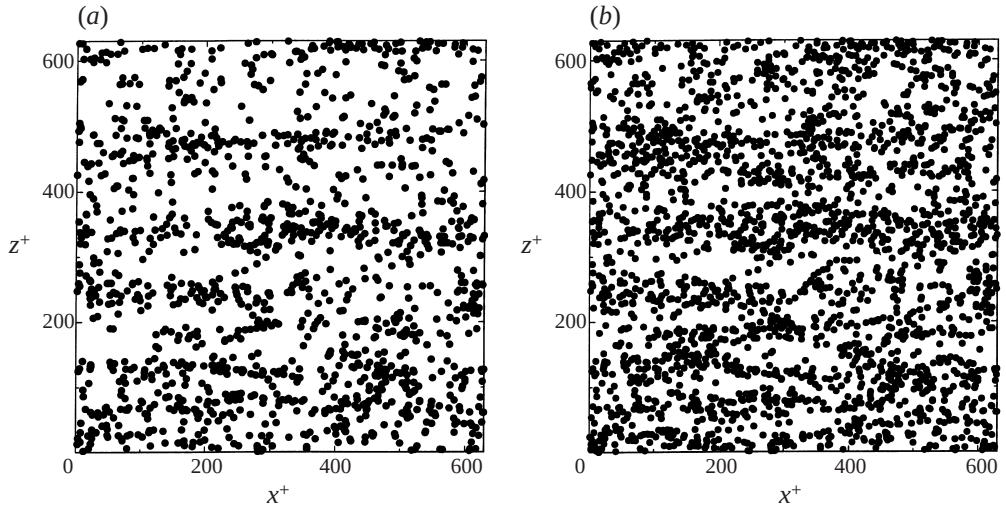

FIGURE 15. Distribution of the initial locations of deposited particles in the (x, z)-plane: (*a*) $d = 15\,\mu$m, (*b*) $25\,\mu$m.

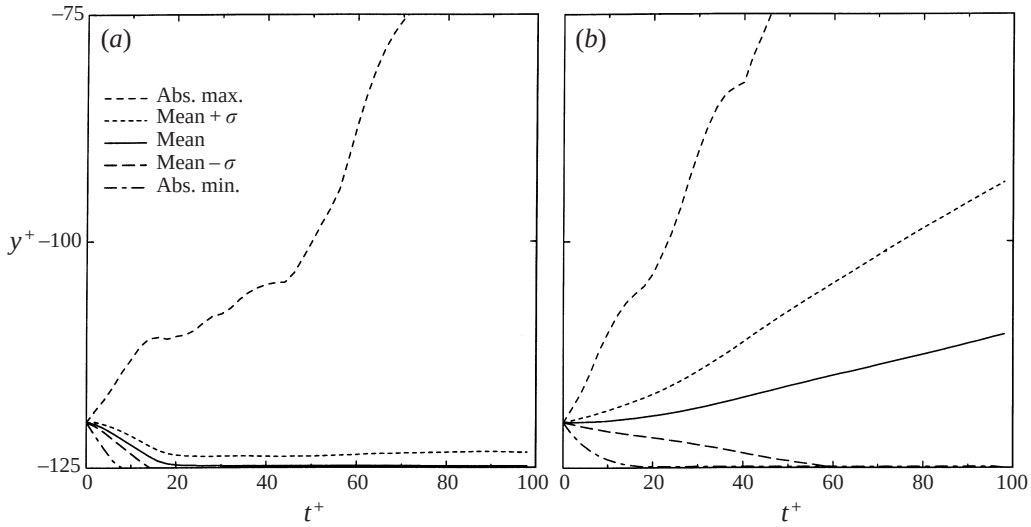

FIGURE 16. Particle trajectory statistics for $d = 30\,\mu$m in a horizontal duct for $u^* = 0.3\,\mathrm{m\,s^{-1}}$ and (*a*) g in the flow direction and (*b*) $g = 0$.

In the absence of gravity, figure 16(*b*) shows that the mean path of particles moves away from the lower wall. As noted before, gravitational sedimentation becomes a major mechanism for particle deposition in horizontal ducts. Unlike the vertical duct case, the maximum particle path shows a noticeable difference due to the presence of gravity. This is because the gravitational force affects the entire region and reduces the maximum distance that particles move away from the wall.

6. Conclusions

In this work, the effect of gravity and its direction on particle transport and deposition in a turbulent channel flow are studied. The flow field is generated by a direct

numerical simulation of the Navier–Stokes equation with the aid of a pseudospectral method. Ensembles of particle trajectories under various gravity conditions are evaluated and statistically analysed. The numerical simulation results for various cases are compared with the available experimental data, earlier simulation results and empirical model predictions. Based on the present results, the following conclusions may be drawn:

(i) In the region near the wall, the mean streamwise velocity has a roughly periodic variation in the spanwise direction with the separation of adjacent high-speed (or low-speed) regions being about 100 wall units.

(ii) The locations of high-speed axial streams correspond to the regions in which the flow moves toward the wall and the low-speed axial streams coincide with the regions in which the flow moves away from the wall.

(iii) The coherent vortical structure of the near-wall turbulent flow plays an important role in the particle deposition process.

(iv) For large particles, the lift and drag forces play a dominant role in particle transportation and deposition, while the Brownian force significantly affects the dispersion of submicrometre particles.

(v) Gravity affects the particle deposition process in a vertical duct through the lift force and through direct sedimentation in a horizontal duct.

(vi) The deposition velocity varies slightly as the density ratio changes for both vertical and horizontal ducts.

(vii) The simulation results are in close agreement with the empirical model predictions, earlier simulation results and the experimental data.

6.1. *Vertical duct*

(viii) The non-dimensional deposition velocity is enhanced when gravity is in the direction of flow, and it is reduced when gravity is opposing the flow direction.

(ix) The effect of gravity on particle deposition rate strongly depends on the magnitude of flow shear velocity. The effect of gravity direction becomes significant for shear velocity less than $0.1\,\mathrm{m\,s^{-1}}$.

(x) In the near-wall region, the mean slip velocity in the streamwise direction due to gravity and its direction increases as shear velocity decreases. For high shear velocities, the mean slip velocity changes only slightly for upward or downward flows; and particles usually move faster than the fluid near the wall in the streamwise direction.

6.2. *Horizontal duct*

(xi) The non-dimensional deposition velocity increases sharply due to gravitational sedimentation effects, and the magnitude of increase is much higher than the corresponding changes for the downflow condition in a vertical channel.

(xii) For horizontal ducts, the non-dimensional deposition velocity varies more significantly with the magnitude of shear velocity than that for vertical channels.

The authors would like to thank Professor John B. McLaughlin and Dr Mehdi Soltani for many helpful discussions. This work was supported by the US Department of Energy under Grant DE-FG26-99FT-40584 and New York State Science and Technology Foundation through the Center for Advanced Material Processing (CAMP) of Clarkson University. The use of the Supercomputer Facility of the San Diego is also gratefully acknowledged.

REFERENCES

Ahmadi, G. 1993 Overview of digital simulation procedures for aerosol transport in turbulent flows. In *Particle in Gases and Liquids 3: Detection, Characterization, and Control* (ed. K. L. Mittal), p. 1. Plenum.

Anderson, R. J. & Russell, T. W. F. 1970 Film formation in two-phase annular flow. *AIChE J.* **16**, 109–123.

Brooke, J. W., Kontomaris, K., Hanratty, T. J. & McLaughlin, J. B. 1992 Turbulent deposition and trapping of aerosols at a wall. *Phys. Fluids* A **4**, 825–834.

Cleaver, J. W. & Yates, B. 1973 Mechanism of detachment of colloid particles from a flat substrate in turbulent flow. *J. Colloid Interface Sci.* **44**, 464–474.

Cleaver, J. W. & Yates, B. 1975 A sublayer model for deposition of the particles from turbulent flow. *Chem. Engng. Sci.* **30**, 983–992.

Cleaver, J. W. & Yates, B. 1976 The effect of re-entrainment on particle deposition. *Chem. Engng Sci.* **31**, 147–151.

Fan, F.-G. & Ahmadi, G. 1993 A model for turbulent deposition of particles in vertical ducts with smooth and rough surfaces. *J. Aerosol Sci.* **24**, 45–64.

Fichman, M., Gutfinger, C. & Pnueli, D. 1988 A sublayer model for turbulent deposition of aerosols. *Aerosol Sci.* **19**, 123–136.

He, C. & Ahmadi, G. 1999 Particle deposition in a nearly developed turbulent duct flow with electrophoresis. *J. Aerosol Sci.* **30**, 739–758.

Hinds, W. C. 1982. *Aerosol Technology*. Academic.

Hinze, J. O. 1975. *Turbulence*. McGraw-Hill.

Kim, J., Moin, P. & Moser, R. 1987 Turbulent statistics in fully developed channel flow at low Reynolds number. *J. Fluid Mech.* **177**, 133–166.

Li, A. & Ahmadi, G. 1993 Deposition of aerosols on surfaces in a turbulent channel flow. *Intl J. Engng Sci.* **31**, 435–445.

McCoy, D. D. & Hanratty, T. J. 1977 Rate of deposition of droplets in annular two-phase flow. *Intl J. Multiphase Flows* **3**, 319–331.

McLaughlin, J. B. 1989 Aerosol particle deposition in numerically simulated turbulent channel flow. *Phys. Fluids* A **1**, 1211–1224.

Marcus, P. S. 1984 Simulation of Taylor–Couette flow. Part 1. Numerical methods and comparison with experiment. *J. Fluid Mech.* **146**, 45–64.

Montgomery, T. L. 1969 Aerosol deposition in a pipe with turbulent air flow. DSc dissertation, University of Pittsburgh.

Niederschulte, M. A., Adrian, R. J. & Hanratty, T. J. 1990 Measurements of turbulent flow in a channel at low Reynolds numbers. *Exp. Fluids* **9**, 222–230.

Ounis, H. & Ahmadi, G. 1989 Motions of small rigid sphere in a simulated random velocity field. *ASCE J. Engng Mech.* **115**, 2107–2121.

Ounis, H. & Ahmadi, G. 1990 Analysis of dispersion of small spherical particles in a random velocity field. Trans. ASME. *J. Fluids Engng* **112**, 114–120.

Ounis, H., Ahmadi, G & McLaughlin J. B. 1991 Dispersion and deposition of Brownian particles from point sources in a simulated turbulent channel flow. *J. Colloid Interface Sci.* **147**, 233–250.

Ounis, H., Ahmadi, G. & McLaughlin, J. B. 1993 Brownian particle deposition a directly simulated turbulent channel flow. *Phys. Fluids* A **5**, 1427–1432.

Papavergos, P. G. & Hedley, A. B. 1984 Particle deposition behavior from turbulent flows. *Chem. Engng Res. Des.* **62**, 275–295.

Pendinotti, S., Mariotti, G. & Banerjee, S. 1992 Direct numerical simulation of particle behavior in the wall region of turbulent flows in horizontal channels. *Intl J. Multiphase Flow* **18**, 927–941.

Rashidi, M., Hetsroni, G. & Banerjee, S. 1990 Particle-turbulence interaction in a boundary layer. *Intl J. Multiphase Flow* **16**, 935–949.

Sehmel, G. A. 1973 Particle eddy diffusivities and deposition velocities for isothermal flow and smooth surfaces. *J. Aerosol Sci.* **4**, 125–138.

Smith, C. R. & Schwartz, S. P. 1983 Observation of streamwise rotation in the near-wall region of a turbulent boundary layer. *Phys. Fluids* **26**, 641–653.

Soltani, M. & Ahmadi, G. 1994 On particle adhesion and removal in turbulent flows. *J. Adhesion Sci. Technol.* **8**, 763–785.

Soltani, M. & Ahmadi, G. 1995 Direct numerical simulation of particle entrainment in turbulent channel flow. *Phys. Fluids* **7**, 647–657.

Squires, K. D. & Eaton, J. K. 1991*a* Measurements of particle dispersion obtained from direct numerical simulations of isotropic turbulence. *J. Fluid Mech.* **226**, 1–35.

Squires, K. D. & Eaton, J. K. 1991*b* Preferential concentration of particles by turbulence. *Phys. of Fluids* A **3**, 1169–1178.

Wood, N. B. 1981*a* The mass transfer of particles and acid vapor to cooled surfaces. *J. Inst. Energy* **76**, 76–93.

Wood, N. B. 1981*b* A simple method for calculation of turbulent deposition to smooth and rough surfaces. *J. Aerosol Sci.* **12**, 275–290.